ELSEVIER

Journal of Power Sources 113 (2003) 422–430

JOURNAL OF POWER SOURCES

www.elsevier.com/locate/jpowsour

Impedance-based non-linear dynamic battery modeling for automotive applications

Stephan Buller*, Marc Thele, Eckhard Karden, Rik W. De Doncker

Institute for Power Electronics and Electrical Drives, Aachen University of Technology, Jaegerstrasse 17-19, D-52066 Aachen, Germany

Abstract

This paper presents a systematic approach to employ electrochemical impedance spectroscopy for determining model structure and parameters of a simulation model for a VRLA battery. It focuses on the interpretation of the impedance data in terms of equivalent circuit models and describes the Matlab/Simulink implementation of the model as well as its time-domain verification. Furthermore, the advantages and limits of the impedance-based model as well as the possible simplifications are discussed.

Keywords: Impedance spectroscopy; VRLA battery; Simulation model; Automotive power system

1. Introduction

Modeling of the dynamical behavior of electrochemical power sources is an important issue in simulation of systems like electric and hybrid vehicles and conventional automotive power systems. In these applications several difficulties arise [1–4]: (i) batteries are not stationary; (ii) electrochemical systems are highly non-linear, and this non-linearity is significant for most power sources under normal operating conditions; (iii) their dynamical behavior depends on many parameters like temperature, state-of-charge (SOC), etc.

Electrochemical impedance spectroscopy (EIS) provides a unique tool for the analysis of the dynamic behavior of batteries. Compared to step-response methods, harmonic small-signal excitation allows for a direct measurement of system response in any working point. The precision of impedance measurements is not limited by the non-linearities or the long relaxation times, which are typical for electrochemical systems. Battery models can be obtained whose elements are closely related to physico-chemical processes.

To obtain simulation models, impedance spectra were recorded systematically for several electrochemical storage systems, e.g. supercapacitors [5], Li-ion batteries and VRLA batteries. Since the latter batteries are most important for near-term automotive applications, they are the main focus of this paper.

2. Impedance spectra of a 36 V AGM battery

The laboratory instrumentation which is needed for high-precision impedance measurements on batteries was developed at ISEA several years ago and is still being further improved. With the so called ISEA ''EISmeter'', it is possible to measure impedances at frequencies from 6 kHz down to frequencies as low as 10 μHz with very high accuracy [2,3]. During an impedance measurement, a small ac current flows through the battery under investigation and the ac voltage response is measured. Furthermore, a superimposed dc (charge or discharge) current defines the overall working point of the battery.

Since battery operation in a (mild, soft or full) hybrid electric vehicle cannot be well described by continuous charge or discharge processes, impedance measurements during dc microcycles have been introduced [2,3]. Starting from a given SOC, the battery is discharged by approximately 5% of its nominal capacity with a defined dc current, and then immediately recharged with the same dc current magnitude for the same time. One impedance spectrum is recorded during the discharge period, one during the charge period. Such microcycles can be repeated several times. It

* Corresponding author. Tel.: +49-241-8096922; fax: +49-241-8092203.
E-mail address: bu@isea.rwth-aachen.de (S. Buller).
URL: http://www.isea.rwth-aachen.de

0378-7753/02/$ – see front matter
PII: S0378-7753(02)00558-X

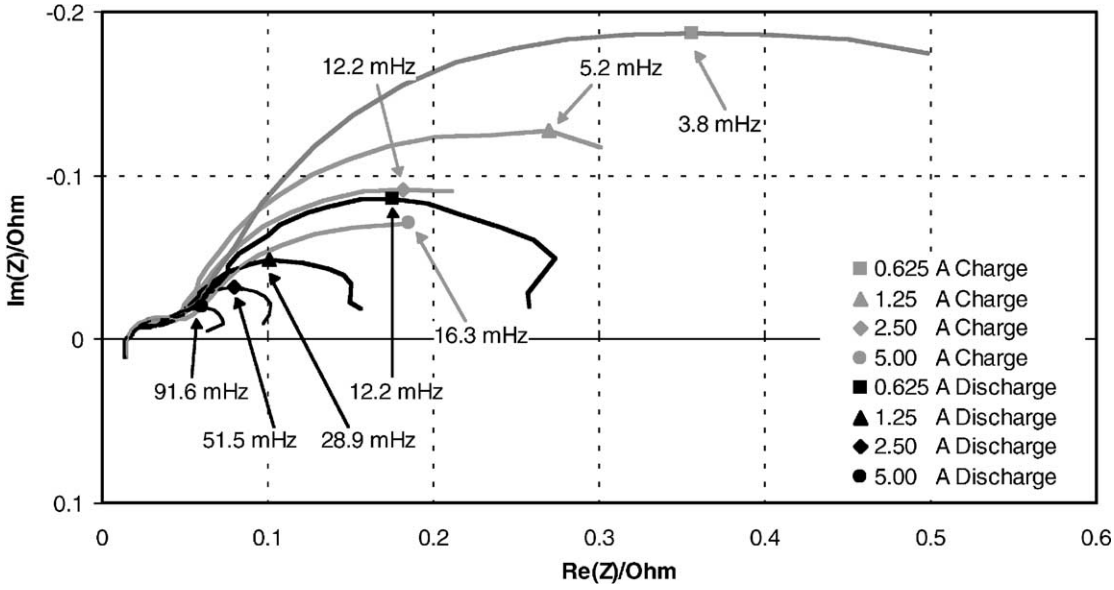

Fig. 1. Impedance spectra of a 36 V AGM battery designed for the 42 V PowerNet for different charge/discharge currents (SOC = 70%, 25 °C).

turns out that for an automotive battery which is usually operated at an intermediate state-of-charge, called partial state-of-charge (PSOC, e.g. 40% < SOC < 70%), the measured impedances are well reproducible from the second microcycle on, (nearly) irrespective of previous history. Therefore, microcycles with the same dc current offset have been repeated two or three times, and only the last impedance spectrum has been used for the battery model [2,3].

Obviously, due to this way of parameter determination, at the beginning of a ride, the simulated voltage response will slightly differ from the measured battery voltage. However, after some idle-stop cycles which correspond well with the microcycles used for the parameter determination, the battery voltage will be modeled much more precisely.

As an example, Fig. 1 shows measured impedance spectra of the 36 V AGM battery for different superimposed charge and discharge currents at approximately 70% SOC and room temperature during microcycle operation. Only the last microcycle for each charge or discharge current is depicted.

3. Impedance-based battery model

The electric behavior of a battery half-cell can be described in a simplified way using the Randles equivalent circuit (Fig. 2). In the figure, only one electrode is modeled, but apart from different parameter values, the basic model for both electrodes is considered to be the same. The equivalent circuit shows an internal resistance R_i, an inductance L, a capacitance C, a non-linear resistance R and a Warburg impedance $\underline{Z}_W$.

Every battery shows an ohmic resistance R_i which is due to the limited conductance of the contacts, the inter-cell connections, the electrodes and the electrolyte. The ohmic resistance depends on the state-of-charge, on the previous usage of the battery and on its age. The inductance L is simply caused by the metallic connection (top lead) between the poles and the electrodes of the battery [3]. To model the capacitive behavior of the half-cell, a capacitance and a non-linear resistance are employed. Diffusion is represented by the Warburg impedance $\underline{Z}_W$.

When the two half-cell impedance models like the one in Fig. 2 are combined to a complete battery model (depicted in Fig. 3), further modifications and simplifications are required. At first, the two resistances and inductances of the half-cells are represented by one element each. Secondly, the dc voltage of the battery cell has to be added to the model. Thirdly, for real electrochemical systems, the capacitances C should be replaced by more general capacitive

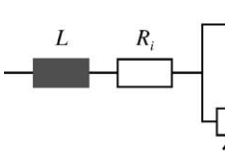

Fig. 2. Equivalent circuit of a battery half-cell.

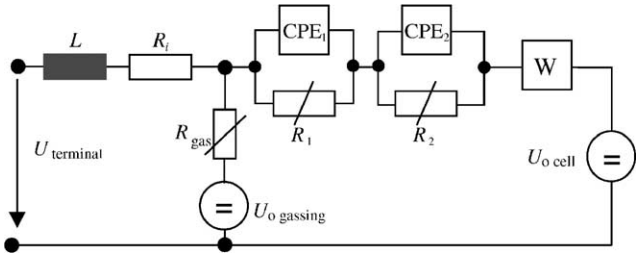

Fig. 3. Simplified equivalent circuit model for a VRLA battery.

elements called constant phase elements (CPE) taking into account the depression of the RC semicircles [3]. The parallel connection of such an element and a resistor is usually referred to as a ZARC element. Furthermore, in [3], it is shown that the influence of the diffusion on the negative electrode is much smaller than its influence on the positive electrode. Therefore, in order to further simplify the combination of the two half-cell models, only one diffusion element is employed for the whole battery cell. Finally, a parallel current path for the side reactions which occur mainly during charging and overcharging has to be realized. Fig. 3 shows the resulting equivalent circuit model used for the interpretation of the measured impedance data.

Theoretically, the diffusion impedance should be located in the faradaic branch of the model (which is the branch of the charge transfer resistance) since the Warburg impedance describes a process which is caused by the electrochemical reaction (''charge transfer'') at the phase boundary between electrode and electrolyte. However, in Fig. 3, the Warburg impedance is crossed by the whole battery current. This simplification allows a much easier implementation and calculation of the model and in general does not lead to significant deviations in the simulation results [1]. If the charge transfer reaction (which is represented by the ZARC element), is much faster than the diffusion process, the Warburg impedance will still be very small for ''high frequency'' currents which are conducted via the capacitive equivalent circuit elements.

For the VRLA battery model, the non-linearity of both ZARC elements, i.e. the non-linearity of the resistances R_1 and R_2 as well as of the capacitive elements A_1 and A_2 (which belong to the two CPE elements) have to be taken into account. Only for the depression factors of the CPE elements (ξ_1 and ξ_2) is linearity assumed, i.e. $\xi_1, \xi_2(I) = \text{const}$. From a physical point of view, the non-linearity with current should rather be regarded as a non-linearity with the corresponding dc potential, but since there is a definite relation between the dc potential and dc current, the non-linearity can also be described as a function of current. This way of expressing corresponds well to the galvanostatic approach for the impedance measurements (with the superimposed dc current) and does not violate universal validity.

For the determination of all the model parameters from the measured impedance spectra a trial version of a fitting software ''Multiple Electrochemical Impedance Spectra Parameterization (MEISP+)'' by Kumho Chemical Laboratories (Korea) has been employed [6]. This software tool facilitates the parameter fitting, but in principle any software tool which allows minimizing the error between a model and measured values (e.g. MS Excel) can be employed.

As an example, in the following paragraphs, the non-linearity of the resistances R_1 and R_2 is discussed. The non-linearity of R_1, which is the resistance of the first ZARC element, is depicted in Fig. 4 for a state-of-charge of 70%. The values for R_1 are determined by a least-square fitting algorithm from the measured impedance spectra. In order to

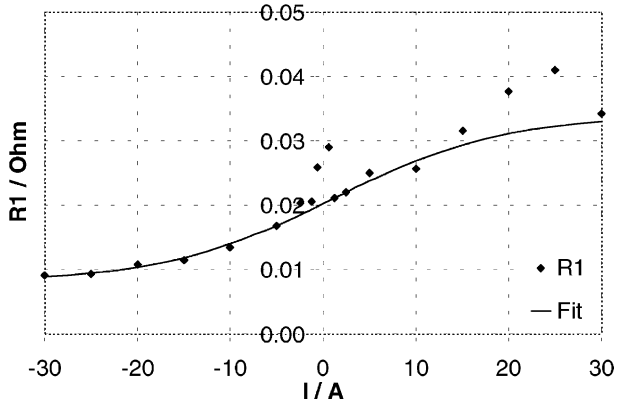

Fig. 4. Non-linearity of the resistance R_1 of the first ZARC element (SOC = 70%, 25 °C).

model the non-linearity, an appropriate approximation curve (called ''Fit'' in Fig. 4) was chosen to represent the received values of R_1. Since this resistance obviously does not show Butler–Volmer behavior, the equation for the approximation of the current dependency of R_1 was chosen phenomenologically according to Eq. (1).

$$R_1(I_{R_1}) = a + b\tanh(c(I_{R_1} + d)) \tag{1}$$

Eq. (1) is employed to represent a linear resistance for discharge currents and a higher linear resistance for charge current as well as a smooth transition between both regions. The four new model parameters (a, b, c and d) are determined by another least-square fitting procedure and are stored in a two-dimensional look-up table. This look-up table takes into account the dependency of the model parameters on the battery temperature and on its state-of-charge.

The non-linearity of R_2 (also determined from the impedance measurements of the whole battery, i.e. 18-battery cells in series) is depicted in Fig. 5. The resistance R_2 shows Butler–Volmer behavior. For one battery cell, the relation between current and the cell's overpotential η is given by Eq. (2):

$$I = I_0\left[\exp\left(\alpha n\frac{\eta}{U_T}\right) - \exp\left(-n(1-\alpha)\frac{\eta}{U_T}\right)\right] \tag{2}$$

with $U_T = 0.026$ V (at 298 K) and $n = 2$.

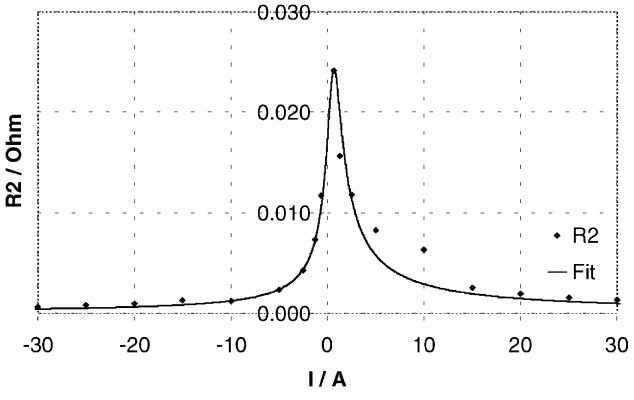

Fig. 5. Non-linearity of the resistance R_2 of the second ZARC element (SOC = 70%, 25 °C).

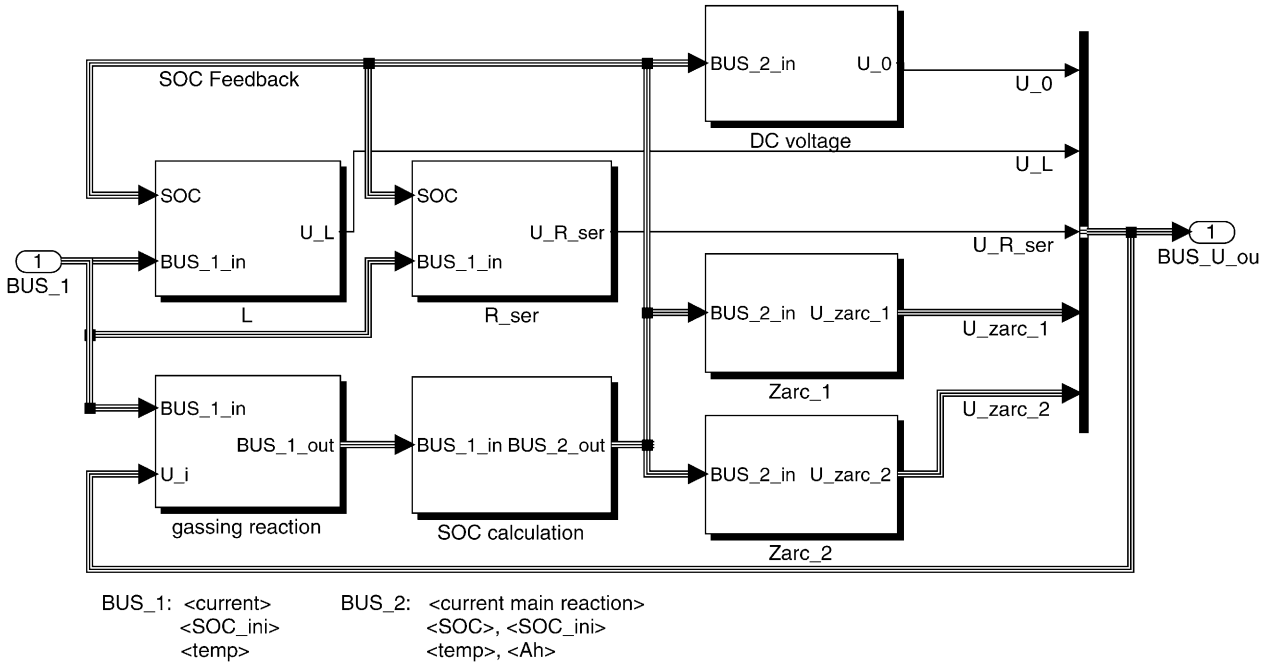

Fig. 6. Topology of the Simulink battery model.

The two parameters I_0 and α are also determined by means of a least-square fitting algorithm and are stored in a look-up table. Again, the look-up table takes into account the dependencies of these parameters on state-of-charge and temperature. The parameter determination of I_0 and α is more difficult than the determination of the other model parameters because the resistance R_2 has to be calculated by differentiating the inverse function of Eq. (2).

After the analysis of the two resistive elements, the capacitive elements (A_1 and A_2) shall be briefly discussed. The values for these elements were determined from the impedance spectra, too. However, during the verification measurements, it was found that an increased value for A_2 led to better simulation results for all test profiles. Therefore, the original parameter A_2 was accordingly modified (about doubled). The reason why the larger value of A_2 led to better simulation results is currently investigated. For example, the influence of the depth of discharge of the microcycles performed during the impedance measurements is analyzed.

4. Matlab/Simulink implementation

Fig. 6 shows the Simulink realization of the general model topology of the VRLA battery which has been presented in Fig. 3. The input quantities of the model are battery current, initial state-of-charge and battery temperature. The primary simulation result is the battery's terminal voltage during dynamic current profiles. Since the impedance spectra in Fig. 1 do not show an obvious influence of diffusion, the Warburg element is neglected in the current version of the simulation model. In the next section of the paper, several verification measurements will show, that this significant simplification is acceptable provided that the use of the model is kept restricted to microcycle operation. However, as mentioned above, the typical load patterns of an automotive battery in PSOC correspond well to the microcycles, which have been used for the parameterization of the model.

5. Verification and discussion

In this section, some verification measurements of the simulation model are presented. At first, Fig. 7 shows a measured and a simulated voltage profile which belong to repeated discharge pulses of −5, −50, −200 and −500 A with zero current periods in between. The measured voltage values show excellent agreement with the simulated voltage profile.

In the next step, the voltage response on a combined charge and discharge current profile is analyzed (Fig. 8). The current profile corresponds to a profile measured during city driving in a 42 V demonstrator vehicle. At first, the engine is started (−500 A, 0.2 s). The cranking sequence is followed by a launch assist sequence (−105 A, 2.8 s) and a short recharge period (e.g. recuperative braking, +35 A, 2.5 s). Then, another electric boost sequence is simulated and finally, the battery is charged again. Although, especially for the charge periods, the differences between the measured and the simulated voltage profile are more pronounced for this combined profile than for the simple discharge profile, the agreement between the two curves is still very good.

Finally, in Fig. 9, the voltage behavior of the battery during a full drive cycle is compared. For this comparison,

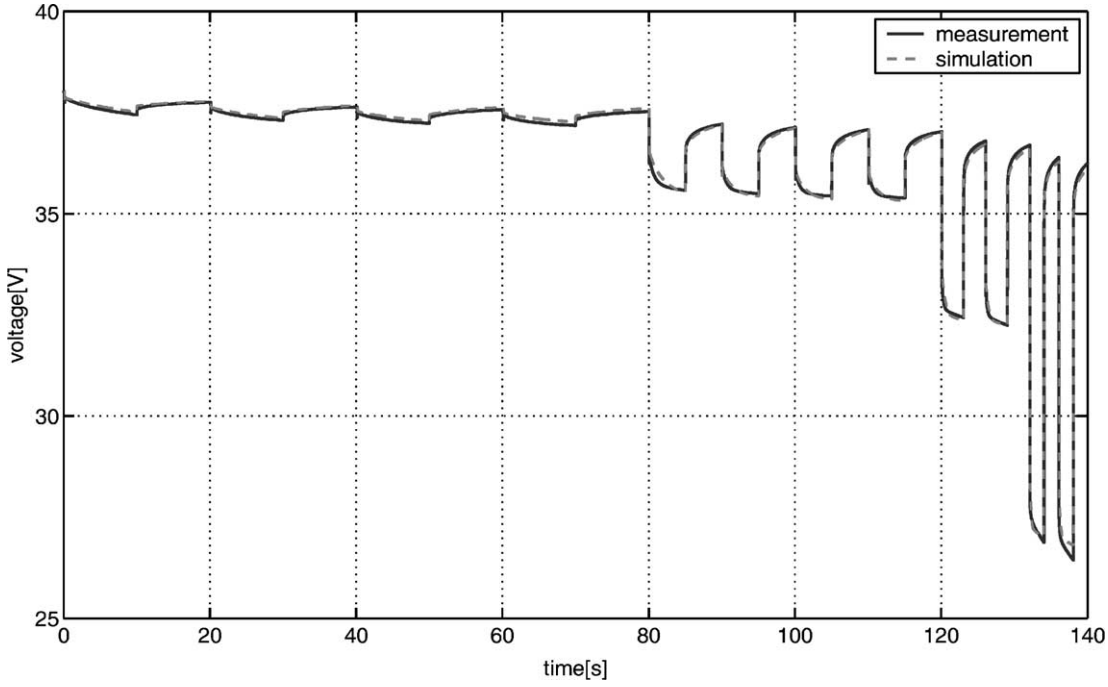

Fig. 7. Discharge profile for the verification of the simulation model (SOC = 70%, 25 °C).

the Federal Urban Driving Schema (FUDS) drive cycle has been translated into a realistic mild-hybrid electric charge/discharge profile for the 36 V VRLA battery (see Table 1). Again, especially during the recuperation periods, the simulated data differs from the measured data. Nevertheless, the simulated voltage profile still fulfills the demands on accuracy for any kind of system simulation.

The most important reason for the deviation during the recuperation periods is due to the nature of the VRLA battery itself, especially due to its (over-) charging behavior. At about 70–80% SOC, the charge acceptance of the battery (at least for some of the 18 cells in series) decreases and the positive electrode goes into overcharge, i.e. water breaks down to form oxygen gas (and hydronium ions). The gas

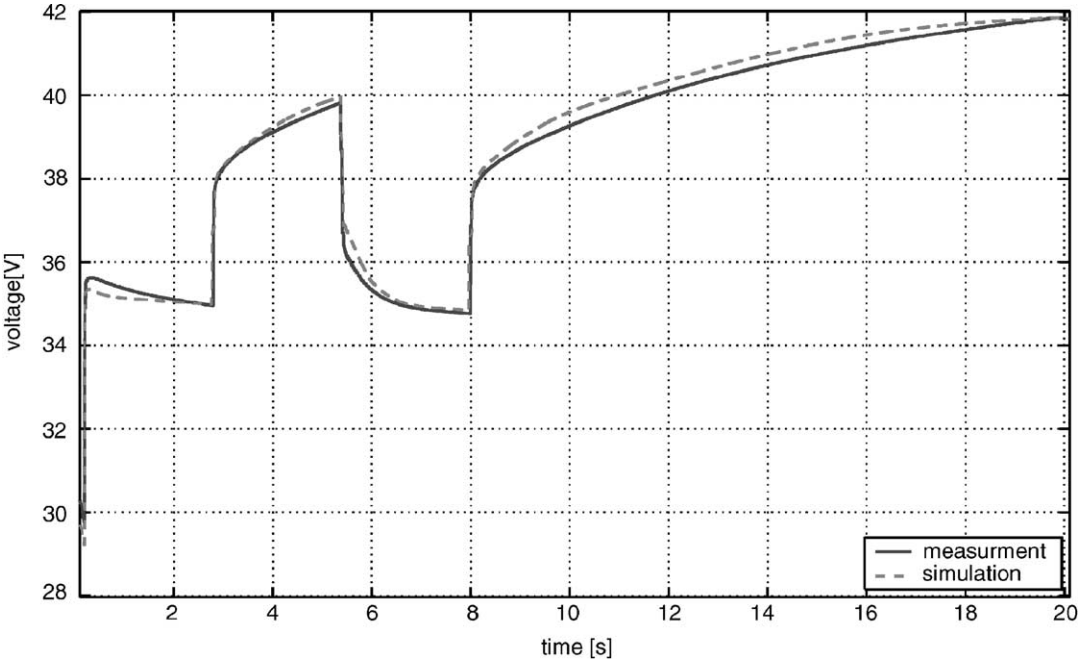

Fig. 8. Cranking, boost + recharge verification profile (SOC = 70%, 25 °C).

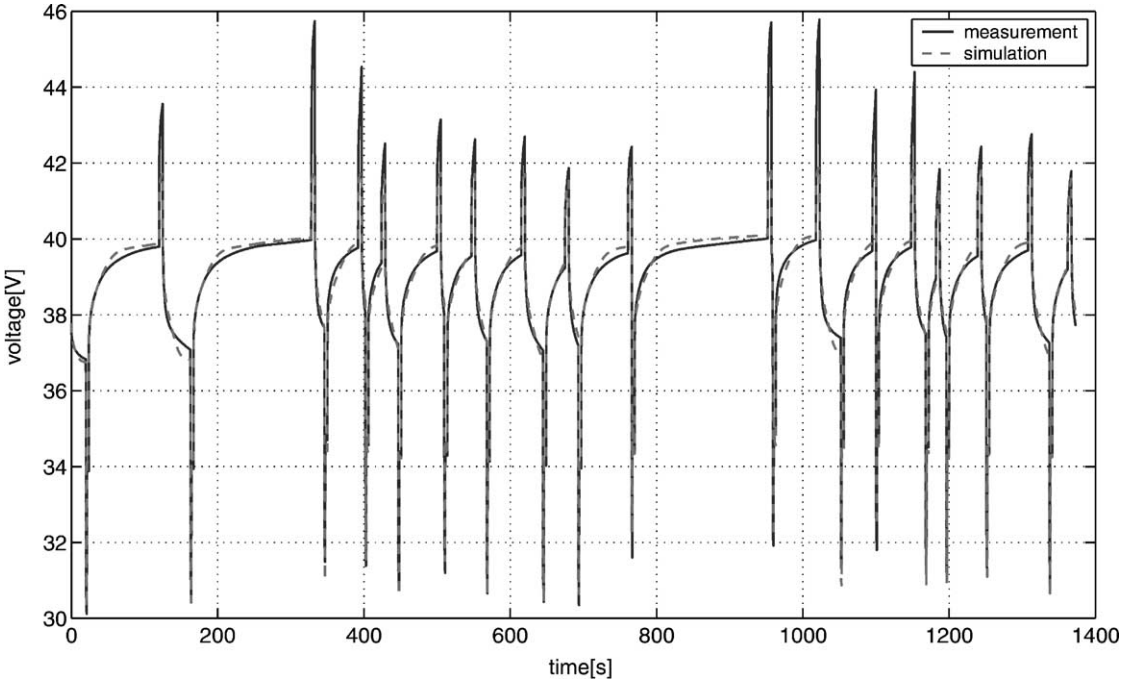

Fig. 9. Electric load profile derived from FUDS drive cycle (SOC = 70%, 40 °C).

forces electrolyte and water out of the positive active material pores and begins the creation of gas paths through the separator mat [7]. However, it takes some time (depending on the battery's age, previous treatment, temperature etc.) until the oxygen reaches the negative electrode where it immediately recombines. The oxygen-recombination drags down the potential of the negative electrode. Therefore, in order to avoid a too-pronounced depolarization of the negative electrode, the efficiency of the oxygen cycle is kept intentionally lower than 100%. Even when the oxygen recombination is in full progress, the resulting (over-) charging potential is somewhere between the flooded and the ideal recombination behavior, depending on the acid saturation of the separator, i.e. depending on the electrolyte volume which again depends on the production process and on the battery's age.

These effects explain the general difficulty to simulate the voltage response of a VRLA battery during (high current) charging at relatively high states-of-charge. To further demonstrate the above mentioned problems from "an impedance point of view", Fig. 10 shows repeated microcycles experiments at a state-of-charge of 70% with a charge current of approximately 1 C. Obviously, the impedance of the microcycle charge spectra decreases from cycle to cycle before it stabilizes when the oxygen cycle has reached its quasi-stationary condition. The choice, which of these microcycles should be used for the simulation model, is more or less arbitrary but has a strong influence of the simulated charging voltage. In our case, we chose the smallest impedance (last spectrum) for the parameter calculation, which explains the rather low simulated charging voltage. However, the strong dependency of the (over-) charging behavior of the VRLA battery (which consists of a series connection of many cells) on the battery's previous usage cannot be completely modeled by means of the presented impedance-based approach.

Table 1
Electric charge/discharge profile derived from FUDS drive cycle

Operation	Power (W)	Duration
Cranking	10,000	1 s
Boost	3500	3 s
Recuperation	3500	5 s
Standstill 42 V	500	Standstill
Driving 42 V	1000	Driving
Load 12 V	300	Always
Charge	1885	If possible

6. Possible simplifications of the model

One of the key ideas of impedance-based modeling of batteries is to achieve a reasonably good simulation model without spending much computing time for the simulation, at least less time than a finite element simulation would need. Thus, it is interesting to discuss possible simplifications of the simulation model in order to compare the gain in time with the corresponding loss in accuracy.

The first simplification to be analyzed is the neglect of the depression of the capacitive semicircles, which alone reduces the simulation time by more than 75%. For many

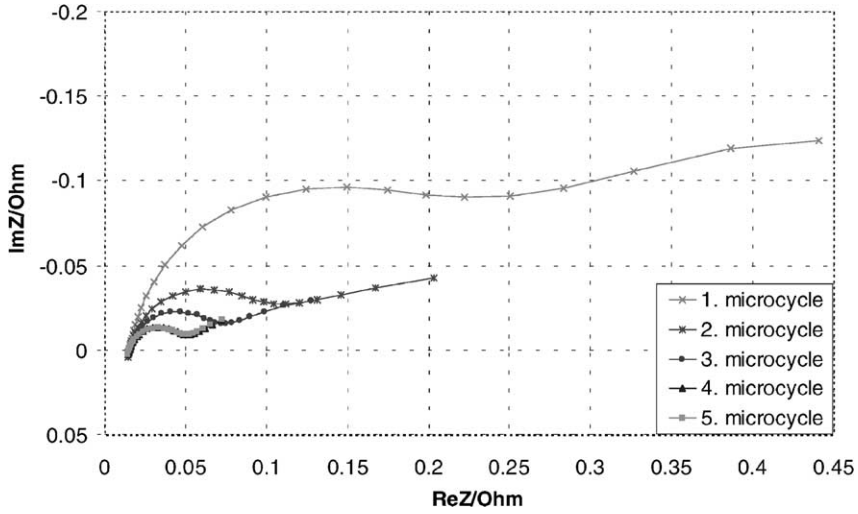

Fig. 10. Repeated microcycles at 75% SOC, charge current 1 C.

applications, this gain in time could be more important than the loss in accuracy.

Fig. 11 shows the described simplification (RC circuit instead of the ZARC element) in the complex plane representation. The diameter of the semicircle as well as its characteristic frequency (frequency of the $|\mathrm{Im}(Z)| = \max.$) are kept unchanged for the RC circuit as well as for the ZARC element. Obviously, for very high frequencies as well as for ultra low frequencies (dc behavior) the impedance of the ZARC element and the RC element show very similar behavior, whereas the impedance shows remarkable deviations for intermediate frequencies. These deviations lead to errors in the dynamic voltage response for an imposed current profile (see Fig. 12). However, the difference between the two

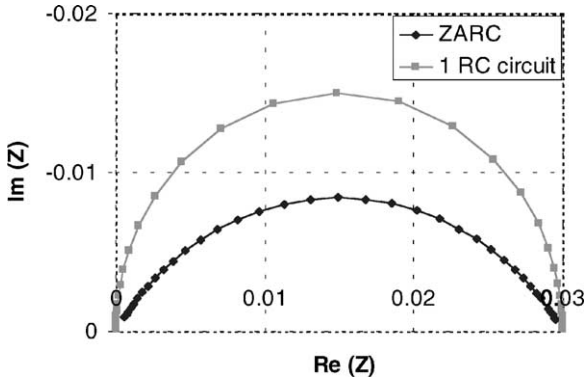

Fig. 11. Approximation of a ZARC element with one (non depressed) RC circuit.

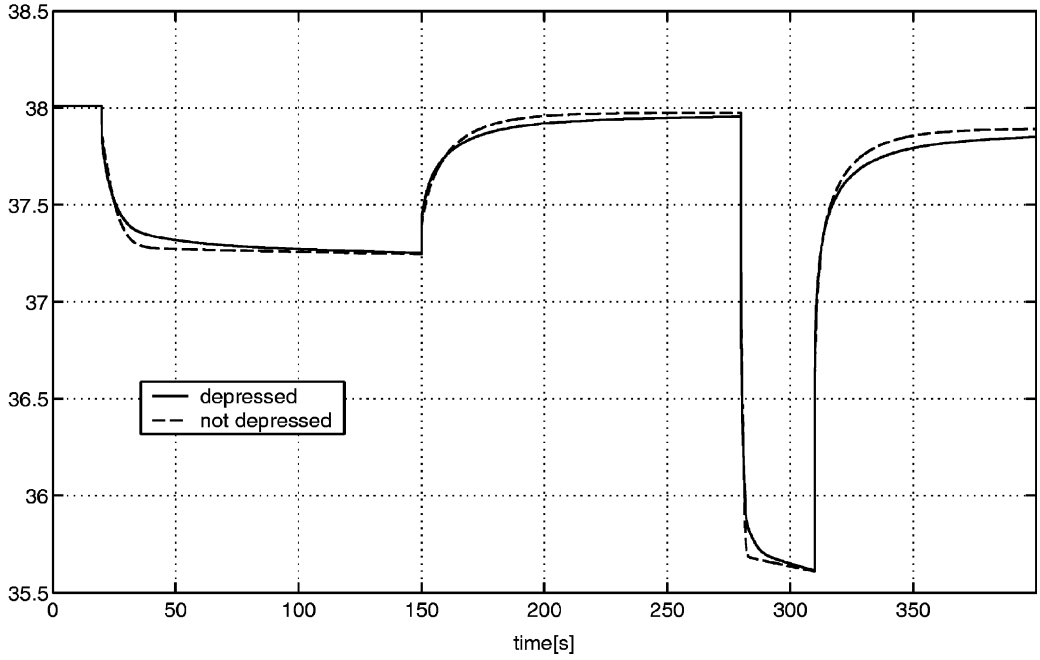

Fig. 12. Comparison of the voltage response of the two simulation models (with and without modeling the depression of the semicircles) on two current steps (first: 0, −5, 0 A; second: 0, −50, 0 A).

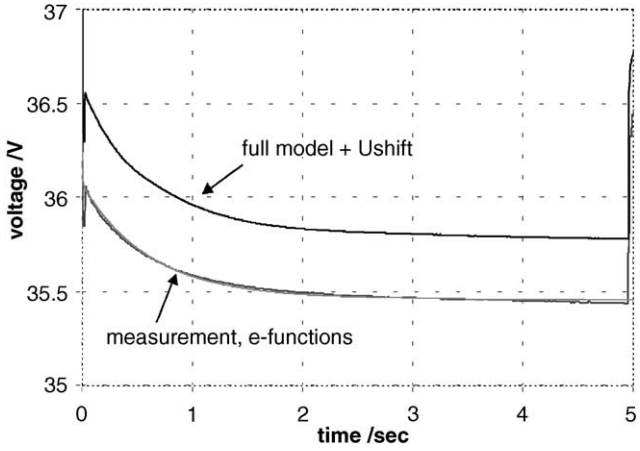

Fig. 13. Comparison of the voltage response of different models (two exponential functions vs. the proposed full simulation model) and the measured voltage (current steps 0, −50, 0 A).

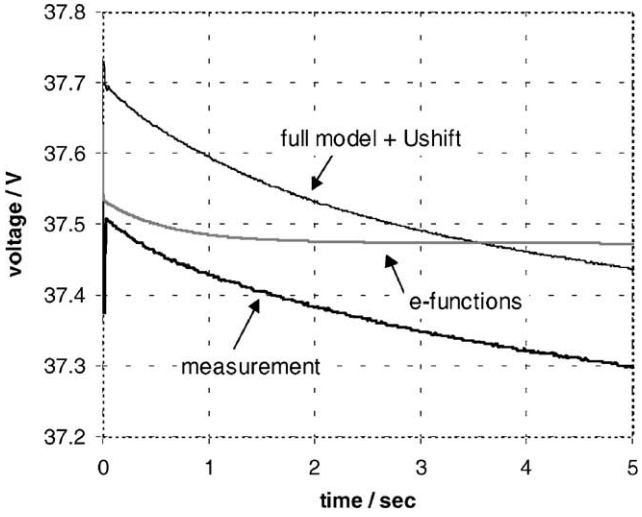

Fig. 14. Comparison of the voltage response of the before-mentioned simulation models on a different current step (0, −5 A).

models is rather small and, furthermore, disappears for low frequencies (i.e. long time periods). Due to the non-linearity of the charge transfer resistance, the deviations disappear faster for high currents, than for lower ones.

In a further step of simplification, the full (non-linear) simulation model is compared to a linear approximation of the battery's voltage response. Since a battery cell consists of two electrodes, two exponential functions are chosen for the time-domain approximation. The four parameters of these exponential functions (R_1, R_2, C_1 and C_2) are determined for a 0 A → −50 A current pulse and are then kept constant for all currents (i.e. linearity is assumed). Fig. 13 shows the best approximation of the voltage response obtained with two exponential functions compared with the voltage response of the full simulation model and also compared with the measured data. In the figure, a dc offset (U_{shift}) has been added to the simulated data of the full model in order to allow for a visual separation of the three nearly identical curves. Obviously, the approximation, by means of two simple exponential functions, also leads to a very good representation of the measured voltage profile.

Now, the parameters are kept constant and both models (the simplified model and the full simulation model) are used to predict the voltage response on a different current step. For this comparison, the current step 0 A → −5 A has been chosen. Now, Fig. 14 clearly shows the very significant deviations between the simple exponential model and the full simulation model as well as the measured data, respectively. Obviously, a linear model is not sufficient to describe the behavior of the battery.

Concluding the discussion about the simplified simulation models, it can be summarized, that the representation of the non-linearity is a crucial part of the battery model which cannot be neglected. If simulation time has to be shortened and if small deviations in the dynamic voltage response of the model are acceptable, a non-depressed representation of the two ZARC elements is suggested.

7. Conclusions and outlook

This paper describes an impedance-based simulation model of a 36 V AGM battery. A systematic approach to employ impedance spectroscopy for determining both model structure and model parameters, is presented. The new Matlab/Simulink model can be used in simulating the voltage response of automotive power sources during highly dynamic current profiles in PSOC operation, e.g. during idle-stop driving in city traffic. The first simulation results that have been achieved with the new model are promising.

In the future, it would be very interesting to parameterize the proposed impedance-based battery model also for a more advanced type of batteries (e.g. a Li-ion battery). First experiments showed that the model topology as well as the measuring procedure should allow for an easy adaptation to these types of batteries.

Acknowledgements

The authors wish to thank Dr. D. Kok and Dr. L. Gaedt from the Ford Research Center Aachen (FFA) for many valuable discussions and, furthermore, wish to thank Ford Motor Company for financially supporting the presented work.

References

[1] P. Mauracher, Modellbildung und Verbundoptimierung bei Elektrostraßenfahrzeugen, Dissertation, RWTH Aachen, 1996.

[2] E. Karden, S. Buller, R.W. De Doncker, A method for measurement and interpretation of impedance spectra for industrial batteries, in: Proceedings of the Labat'99 Conference, Sofia, Bulgaria, J. Power Sources 85 (2000) 72–78.

[3] E. Karden, Using low-frequency impedance spectroscopy for characterization, monitoring and modeling of industrial batteries, Dissertation, RWTH Aachen, 2001.
[4] E. Karden, S. Buller, R.W. De Doncker, A frequency-domain approach to dynamical modeling of electrochemical power sources, Electrochimica Acta 47 (2002) 2347–2356.
[5] S. Buller, E. Karden, D. Kok, R.W. De Doncker, Modeling the dynamic behavior of supercapacitors using impedance spectroscopy, in: Proceedings of the IEEE IAS Meeting, Chicago, 2001.
[6] Korea Kumho Petrochemical Co. Ltd., Multiple electrochemical impedance spectra parameterization MEISP+, User Manual, Kumho Chemical Laboratories, Yuseong, Taejon, Korea, 2001.
[7] R. Nelson, Valve regulated lead acid batteries, Tutorial at AABC'02, Advanced Automotive Battery Conference, Las Vegas, USA, February 2002.